



Labdane and Norlabdane Diterpenoids from the Rhizomes of *Amomum villosum* var. *xanthioides* with Anti-inflammatory and α -Glucosidase Inhibitory Activities

Hong Yin,[†] Wen-Jia Dan,[†] Bo-Yi Fan,[‡] Chao Guo,[⊥] Kui Wu,[§] Ding Li,[†] Kui-Feng Xian,[†] Gennaro Pescitelli,[^]  and Jin-Ming Gao*[†] 

[†]Shaanxi Key Laboratory of Natural Products & Chemical Biology, College of Chemistry & Pharmacy, Northwest A&F University, Yangling 712100, Shaanxi, People's Republic of China

[‡]School of Pharmacy, Nantong University, Nantong 226001, Jiangsu, People's Republic of China

[⊥]School of Pharmacy, Xinxiang Medical University, Xinxiang 453003, Henan, People's Republic of China

[§]Department of Chemistry, University at Albany, State University of New York, Albany, New York 12222, USA

[^]Dipartimento di Chimica e Chimica Industriale, Università di Pisa, Pisa, 56124, Italy

ABSTRACT: A novel norditerpene (**1**), two new labdane diterpenes (**2**, **3**) and nine known analogues (**4–12**) were isolated from the rhizomes of *Amomum villosum* var. *xanthioides*. **1** is an unprecedented rearranged tetranorlabdane diterpene, featuring a 6/6/5 fused tricyclic skeleton with an α,β -unsaturated cyclopentenone unit, while **2** is a structurally rare labdane diterpene bearing a five-membered cyclic anhydride. Their structures and absolute configurations were established on the basis of spectroscopic data and quantum chemical ECD calculations. **4** shows remarkable inhibitory activity against nitric oxide production with an IC_{50} value of 2.36 μM , and could also inhibit α -glucosidase activity significantly ($IC_{50} = 9.98 \mu M$).

INTRODUCTION

Amomum villosum Lour. var. *xanthioides* (Wall. ex Bak.) T. L. Wu & Senjen, belonging to the Zingiberaceae family, is widely distributed in southern China, Laos, Vietnam, Cambodia, and Thailand.¹ It is commonly dedicated to traditional Chinese medicine for the treatment of stomach diseases and digestive disorders.^{2,3} The previous investigations indicated that *A. villosum* var. *xanthioides* contains abundant essential oil,⁴ terpenoids,^{5,6} phenols⁵ and flavonoids,⁵ meanwhile it shows anti-cancer,⁷ anti-inflammation,⁸ anti-allergy,⁹ and hepatoprotective effect.¹⁰ Our recent phytochemical investigation on medicinal plants of the *Amomum* genus identified a series of diterpenoids^{11,12} and unusual norditerpenoids.¹³ In our ongoing endeavor to discover structurally interesting and biologically relevant components beneficial for human life and health from the rhizomes of *A. villosum* var. *xanthioides*, an unprecedented rearranged tetranorlabdane diterpene with a 6/6/5 tricyclic skeleton, avxanthin A (**1**), two new labdane diterpenes, avxanthins B (**2**) and C (**3**), together with nine known analogues (**4–12**) were isolated (Figure 1). Herein, we present their isolation and structure elucidation, as well as anti-inflammatory and α -glucosidase inhibitory activities.

RESULTS AND DISCUSSION

Compound **1** was isolated as colorless oil. HRESIMS data (m/z 233.1899 $[M + H]^+$, calcd for $C_{16}H_{25}O$, 233.1899) gave the molecular formula $C_{16}H_{24}O$, corresponding to five degrees of unsaturation. The 1H NMR spectrum displayed three high-field methyl singlets at δ_H 0.85, 0.911 and 0.915. The ^{13}C NMR, DEPT, and HSQC spectra revealed 16 carbons for three methyls, seven methylenes, one methine, and five quaternary carbons (including a ketone carbonyl at δ_C 209.3, two olefinic quaternary carbons at δ_C 138.5 and 172.6, which occupied two degrees of unsaturation).

Above evidence suggested that **1** was a norditerpenoid possessing a tricyclic system. The gross structure of **1** was deduced by analysis of 2D NMR data (HSQC, HMBC, ^1H - ^1H COSY, and ROESY) (Figure 2). In the HMBC spectrum, a methyl singlet at δ_{H} 0.911 (3H, s) ascribable to Me-14, showed significant correlations with a methyl carbon at δ_{C} 21.7 (C-15) and an sp^3 quaternary carbon at δ_{C} 33.3 (C-4), the methyl singlet at δ_{H} 0.915 (3H, s, Me-15) with an sp^3 methylene at δ_{C} 42.8 (C-3) and an sp^3 methine at δ_{C} 48.8 (C-5), the third methyl singlet at δ_{H} 0.85 (3H, s, Me-16) with C-5 (δ_{C} 48.8) and an sp^3 methylene at δ_{C} 42.0 (C-1), as well as H-2b (δ_{H} 1.46, 1H) exhibited correlations with an sp^3 quaternary carbon at δ_{C} 33.9 (C-10). Taking the ^1H - ^1H COSY spin-coupling systems H-1/H-2/H-3 into consideration, a six-membered ring A was ascertained (Figure 1). Furthermore, HMBC correlations from H-9b (δ_{H} 2.00) to two olefinic quaternary carbons at δ_{C} 138.5 (C-7) and 172.6 (C-8), and from H-6a (δ_{H} 2.34) to C-8 indicated that one olefinic bond was placed at C-7/C-8. Again, considering the spin-coupling systems H-5/H-6 in the ^1H - ^1H COSY spectrum and HMBC correlations of H-9b with C-5, C-10 and C-16, another six-membered ring B was constructed to be fused with ring A at C-5/C-10 (Figure 1). Similarly, an sp^3 methylene signals at δ_{H} 2.40 and 2.43 (2H, H-11) showed HMBC correlations with the carbonyl carbon at δ_{C} 209.3 (C-13), and another sp^3 methylene protons at δ_{H} 2.39 (2H, H-12) with C-13, C-8 and C-7. Additionally, the ^1H - ^1H COSY spin-coupling systems H-11/H-12 as well as HMBC correlations of H-9b with C-11 and H-6a with C-13 were also observed. Combining the above information with the degrees of unsaturation, an α,β -unsaturated cyclopentenone unit (ring C) comprised C-7, C-8, C-11, C-12, and C-13 was fused with ring B at C-7/C-8 (Figure 1).

On the basis of ROESY data, correlations between H-5 with Me-14, and between Me-15 with Me-16 indicated the relationship between H-5 and Me-16 to be *trans* (Figure 2). The absolute

configuration was determined by comparison of the calculated and experimental electronic circular dichroism (ECD) spectra. The CD spectrum of compound **1** contained the two typical bands of the enone chromophore, namely a $n-\pi^*$ band with maximum at 310 nm, and a $\pi-\pi^*$ band with maximum at 240 nm corresponding to the strong UV absorption.¹⁴ Because of the five-membered ring, the enone is essentially planar, thus so-called helicity rules can't be employed. However, the presence of a single simple chromophore embedded in a rigid molecular skeleton makes this case, as well as similar ones,¹⁵ ideal for CD calculations. In fact, compound **1** existed as a single conformer, according to density functional theory (DFT) geometry optimizations, shown as inset in Figure 3, which was in accord with NOESY correlations. The CD spectrum calculated for (5*S*,10*R*)-**1** with time-dependent DFT (TD-DFT) at CAM-B3LYP/def2-TZVP level,^{16,17} (including a PCM solvent model for MeOH) matched perfectly the experimental spectrum recorded for (+)-**1** (Figure 3), thus allowing a safe configurational assignment as 5*S* and 10*R*. The similarity factor (SF), which quantifies the similarity between calculated and experimental spectrum, amounted to 0.992. The value of SF for **1** indicated complete match between the spectra. Accordingly, compound **1** was established, and named as avxanthin A.

Compound **2** was obtained as white powder. The molecular formula was deduced as C₂₀H₂₈O₃ by HRESIMS data at m/z 317.2114 [M + H]⁺ (calcd for C₂₀H₂₉O₃, 317.2111), which suggested seven degrees of unsaturation. The ¹H NMR spectrum showed three high-field methyl singlet signals at δ_{H} 0.73, 0.82 and 0.89, and one exocyclic methylene signals at δ_{H} 4.38 and 4.84, which were the characteristics for a labdane diterpene with an *exo*-methylene group at C-8.¹⁸ The ¹³C NMR spectrum indicated that **2** was also a labdane diterpene with an *exo*-methylene (δ_{C} 107.6, C-17) and three methyls (δ_{C} 14.5, C-20; δ_{C} 21.9, C-19; δ_{C} 33.7, C-18). All of the proton and carbon signals (Table 2)

were assigned by 2D NMR spectra (HMQC, HMBC and ROESY). Analysis and comparison of NMR data revealed that the structure of **2** was similar to (*E*)-labda-8(17),12-dien-16,15-olide,¹⁹ except for the five-membered ring system in the side chain. The absence of the oxymethylene in position C-15 and the appearance of a carbonyl carbon signal at δ_C 173.9 were observed, besides the methylene carbon signal at C-14 shifted downfield compared to (*E*)-labda-8(17),12-dien-16,15-olide ($\Delta\delta_C +7.8$), which suggested that the carbonyl group (δ_C 173.9) was assigned to C-15, and a five-membered cyclic anhydride moiety was formed. The deduction was further substantiated by HMBC correlations of H-14 (δ_H 3.26) with C-16 (δ_C 169.6), C-15 (δ_C 173.9), C-13 (δ_C 125.9) and C-12 (δ_C 141.6), and H-12 (δ_H 6.80) with C-16. Moreover, a trisubstituted olefinic proton signal at δ_H 6.80 was observed in ¹H NMR spectrum, and an assignment of the corresponding olefinic bond $\Delta^{12(13)}$ was achieved on the basis of HMBC correlations of H-12 with C-9 and C-16, and H-11 with C-12 and C-13. Absence of ROESY interaction between H-12 and H-14, along with the downfield shift of H-12 (δ_H 6.80) due to the deshielding effect of the carbonyl group at C-16 revealed the olefinic bond $\Delta^{12(13)}$ with an *E* geometry.¹⁹ In addition, ROESY interactions of H-5 with H-9 and Me-18, and Me-19 with Me-20 suggested H-5, H-9 and Me-18 to be α -oriented, and Me-19 and Me-20 to be β -oriented (Figure 4). On the basis of the aforementioned spectroscopic features as well as the total degrees of unsaturation, compound **2** was identified as (*E*)-labda-8(17),12-dien-15,16-dioic anhydride, and named as avxanthin B. The absolute configuration of **2** was determined using the same procedure employed for **1**. The two compounds differ substantially from the viewpoint of ECD spectroscopy, because in **2** the main chromophore – a cyclic α,β -unsaturated anhydride – is essentially planar and attached to the chiral skeleton through a flexible junction. As a consequence, not only compound **2** may assume several different conformations, but the various conformers are associated

with very different ECD spectra from each other. The lowest-energy structure of **2** optimized at ω B97X-D/6-311G+(d,p) level of theory, including SMD solvent model for methanol, is shown in Figure 5 (labelled conf. 1, 60% population). The prevalence of such conformation is substantiated by the NOE observed between H-14 and H-17. However, a second diagnostic NOE between H-1 and H-14 is not expected for the lowest-energy minimum but only for the second most stable one (conf. 2 in Figure 5, 14% population). The ECD spectrum calculated for (5*S*,9*S*,10*S*)-**2** at CAM-B3LYP/def2-TZVP level (including a PCM solvent model for MeOH) was in satisfactory agreement with the experimental spectrum recorded for (+)-**2** (Figure 5). The main discrepancy between the two spectra is the positive experimental ECD band around 210 nm which is missing in the calculation. This may be partly due to an understimation of the population of conformer 2, which displays a positive ECD band in this region. Still, the SF was 0.90 for the calculated absolute configuration and 0.06 for its enantiomer. The absolute configuration of avxanthin B is thus established as (+)-(5*S*,9*S*,10*S*)-**2**.

Compound **3** was isolated as colorless oil. HRESIMS data (m/z 363.2531 [M + H]⁺, calcd for C₂₂H₃₅O₄, 363.2530) gave the molecular formula C₂₂H₃₄O₄. The ¹H NMR data showed three methyl singlets at δ_{H} 0.72 (H-20), 0.82 (H-19), and 0.88 (H-18), and the *exo*-methylene protons (δ_{H} 4.84, 4.40, H-17), which also provided evidence for **3** being a labdane diterpenoid.¹⁸ In ¹H and ¹³C NMR spectra, an ethoxy group was observed for signals at δ_{H} 4.16 (2H, q, $J = 7.0$ Hz, -OCH₂CH₃, H-21) and 1.26 (3H, t, $J = 7.0$ Hz, -OCH₂CH₃, H-22) as well as δ_{C} 61.1 (-OCH₂CH₃, C-21) and 14.3 (-OCH₂CH₃, C-22), respectively. Comprehensive analysis of NMR spectra and comparison with literature data indicated that **3** was analogous to (*E*)-labda-8(17),12-dien-15,16-dioic acid,²⁰ except for the presence of one additional ethoxy group and the chemical shift of C-15 appeared at a

relatively high field ($\Delta\delta_c -6.9$) for **3**. It was deduced that the carboxylic acid located at C-15 was replaced by an ethyl ester, which was further demonstrated by HMBC correlations of H-21 (δ_H 4.16) with C-15 (δ_c 170.7) and C-22 (δ_c 14.3). The ROESY correlation between H-14 and H-11 also confirmed that the double bond $\Delta^{12(13)}$ was an *E* geometry. In addition, ROESY data showed that **3** possessed the same relative configuration as **2** (Figure 4). Accordingly, compound **3** was determined as (*E*)-labda-8(17),12-dien-15-ethyl ester,16-oic acid, and named as avxanthin C. The absolute configuration of this latter compound could not be established by the aforementioned ECD method, because its ECD spectrum was very weak. This is apparently due to the hydrolysis of the anhydride which, though preserving a α,β -unsaturated carboxylate chromophores, adds further flexibility to the molecule which is detrimental for the ECD intensity. Based on the co-occurrence with three compounds whose absolute configuration is established by ECD calculations and share exactly the same chiral moiety, we assign avxanthin C as (+)-(5*S*,9*S*,10*S*)-**3**.

Compound **4** was yellowish oil. HRESIMS provided the molecular formula $C_{20}H_{28}O_3$. The 1H and ^{13}C NMR spectra indicated **4** also be a labdane diterpene. On the basis of spectroscopic data, including HSQC and HMBC data (Figure 4), the planar structure of **4** was identical with that of 16-hydroxylabda-8(17),11,13-trien-15,16-olide.²¹ In this latter reference, compound **4** was isolated as a mixture of C-16 epimers, and its absolute configuration remained undetermined. Compound **4** in our hands shows instead a single set of NMR signals, with no splitting of C-16 or H-16 resonances. This indicated the presence of a single stereoisomer, whose relative and absolute configuration needed to be assigned. To this end, NOESY experiments and ECD calculations were performed.

The relative configuration of **4** was established by ROESY correlations of H-9/H-5, H-5/Me-18, H-6 α (δ_H 1.76)/Me-18, H-6 β (δ_H 1.41)/Me-19, and H-6 β /Me-20, as shown in Figure 4. In addition,

two olefinic protons at δ_{H} 6.62 (H-11) and δ_{H} 6.38 (H-12) were mutually coupled with a large coupling constant of 16.0 Hz, indicating the double bond $\Delta^{11(12)}$ with the *trans* isomerism.²² The observed NOESY correlation of H-14 (δ_{H} 5.91) with H-12 (δ_{H} 6.38) rather than with H-11 (δ_{H} 6.62) revealed that the conjugated dienes system formed by two double bonds $\Delta^{11(12)}$ and $\Delta^{13(14)}$ had the *s-trans* conformation. Unfortunately, ROESY correlations could not be used to safely discriminate between the two possible orientation of the 16-OH group, because of the lack of ROESY correlation between the α,β -unsaturated butyrolactone ring and the bicyclic system. Thus, two different diastereomers were possible, (5*S**,9*S**,10*S**,16*R**) and (5*S**,9*S**,10*S**,16*S**). To assign the absolute configuration and possibly the relative configuration at C-16, TDDFT calculations were run on (5*S*,9*S*,10*S*,16*R*)-**4** and (5*S*,9*S*,10*S*,16*S*)-**4** (or epi-**4**), using the same procedure adopted for **1**. The two diastereomers led both to the correct sign for the π - π^* band of the dienoate chromophore at 260 nm (Figure 6). Around 200 nm, however, epi-**4** displayed a calculated positive CD band with no experimental counterpart, corresponding to the n - π^* transition which was intrinsically more sensitive to the configuration at C-16.²³ As a consequence, the similarity factor (SF) for **4** was 0.996, while for epi-**4** decreased down to 0.885. Compound **4** was then elucidated as (5*S*,9*S*,10*S*,16*R*,11*E*)-16-hydroxyabda-8(17),11,13-trien-15,16-olide.

The remaining known compounds were identified as abda-8(17),13(14)-dien-15,16-olide (**5**),²⁴ (*E*)-abda-8(17),12-dien-16,15-olide (**6**),¹⁹ coronarin-D methyl ether (**7**),²⁵ coronarin-D ethyl ether (**8**),²⁶ 15-hydroxyabda-8(17),13-dien-16,15-olide (**9**),²⁷ (*E*)-abda-8(17),12-dien-15-ol-16-al (**10**),²⁸ (*E*)-14,15,16-trinorabda-8(17),11-dien-13-oic acid (**11**),²² (*E*)-14-hydroxy-15-norabda-8(17),12-dien-16-al (**12**).²²

A review concerning norlabdane diterpenoids obtained from plants of the Zingiberaceae

family^{13,22} suggested that norlabdane diterpenes may be degraded from normal labdane diterpenes.¹³ Consequently, we tentatively proposed a plausible biogenetic pathway of compound **1**, which was originated from compound **6**, outlined in Scheme 1. Compound **6** was proposed to be involved in the double bond migration from $\Delta^{12(13)}$ to $\Delta^{13(14)}$, esterlysis, further oxidation of $\Delta^{13(14)}$ and decarboxylation at C-16, to afford intermediate A. After reduction of the carboxyl group and the following dehydration, intermediate A was converted to intermediate B. Intermediate B might undergo [3,3] sigmatropic rearrangement to produce intermediate C. Via oxidation of the terminal double bond of intermediate C, followed by Friedel-Crafts type cyclization between the carboxyl group and C-7,²⁹ a five-membered ring fused with the decalin nucleus at C-7/C-8 was finally formed. Therefore, from a biogenetic point of view, compound **1** is the first example of unprecedented rearranged tetranorlabdane diterpene with a 6/6/5 fused tricyclic skeleton.

The inhibitory effects of compounds **1–12** on NO production in LPS-induced RAW 264.7 macrophages were tested. Cell viability was determined by the MTT method to find whether inhibition of NO production was due to cytotoxicity of compounds.³⁰ As shown in Table 3, all of the compounds, except **3** and **10**, inhibited NO production to various degrees. Among them, compounds **2** and **4** exhibited significant inhibitory abilities, with IC_{50} values of 11.02 and 2.36 μM , respectively, and compounds **5–9**, **11** and **12** showed moderate inhibitory effects with IC_{50} values of 18.84–31.20 μM , compared to that of the positive control NG-monomethyl-L-arginine (L-NMMA). The results of NO expression indicated that inhibitory activities of normal labdane diterpenes with a five-membered ring between C-15 and C-16 (**2**, **4**, **5**, **6**, **7**, **8** and **9**) were superior to those without (**3** and **10**). Again, labdane diterpenes with 15,16-olide or 15,16-dioic anhydride (**2**, **4** and **5**) displayed stronger activities than those with 16,15-olide (**6**, **7**, **8** and **9**).

Molecular docking approach was employed to investigate the probable binding interactions between compound **4** and iNOS protein, a key enzyme for regulation of NO production in the inflammatory process.³¹ Compound **4**, the most potent NO inhibitor, bound tightly to the active cavity of iNOS with binding energy of -9.13 kcal/mol. As shown in Figure 7, the decalin nucleus moiety of **4** was embedded deeply in the hydrophobic pocket formed by Pro350, Ala351, Val352, Phe369, Trp372 and Tyr373. Moreover, two hydrogen bonds were formed between the hydroxyl group at C-16 of **4** and the carboxyl group of Glu377, as well as between the carbonyl oxygen atom of **4** and the amino of Arg388. On the basis of the detailed interactions of **4** with the key residues, it was concluded that the hydrophobic interactions and hydrogen bonds could play great contributions to the binding of **4** to iNOS. The docking results provided us insight into the protein-ligand interactions, which implied that the possible inhibitory mechanism of NO production of **4** by interaction with targeting residues in the active cavity of iNOS.³²

Compounds **1–12** were also evaluated for α -glucosidase inhibitory activities *in vitro*, using 1-deoxynojirimycin and genistein as positive controls.³³ As a result, at a concentration of $50 \mu\text{M}$, all the isolates showed various degrees of α -glucosidase inhibition, and more than 80% inhibition was observed among compounds **2**, **4–9** (Table 4). The following IC_{50} values of **2**, **4–9** further demonstrated their significant inhibitory effects on α -glucosidase, and compound **4** was the most potent inhibitor with the IC_{50} value of $9.98 \mu\text{M}$ (Table 4). It was noteworthy that the inhibitory activities of **2**, **4–9**, possessing a lactone ring or cyclic anhydride between C-15 and C-16, were much better than those of labdane and norlabdane diterpenes without a five-membered ring moiety formed (compounds **3**, **10–12**). These results suggested that the cyclic motif between C-15 and C-16 of labdane diterpenes might play an important role in the α -glucosidase inhibitory activity.

To further explore the type of inhibition of α -glucosidase activity, kinetic studies were performed on compound **4**. The kinetic type was determined by the Lineweaver–Burk double-reciprocal plots, as depicted in Figure 8, which showed that a set of lines with different slopes and intercepts intersected in the third quadrant. With the concentration of **4** increasing, K_m and V_{max} values both decreased (S5, Supporting Information), and the K_i value was calculated to be $9.50 \pm 0.11 \mu\text{M}$. These results indicated that **4** bound mainly in a single class of inhibition sites on α -glucosidase with a mixed-type manner.³⁴

EXPERIMENTAL SECTION

General Experimental Procedures. Optical rotations were measured with a MCP 300 polarimeter (Anton Paar GmbH, Graz, Austria). The electronic circular dichroism (ECD) spectra were determined with an Applied Photophysics Chirascan spectrometer (Applied Photophysics Ltd., London, UK). UV spectra were performed on Thermo Evolution 300 ultraviolet–visible spectrophotometer (Thermo Electron Corporation, Madison, USA). 1D and 2D NMR spectra (^1H : 500MHz and ^{13}C : 125MHz) were acquired on a Bruker Avance III NMR instrument (Bruker Corporation, Madison, USA). HRESI mass spectra were carried out using a Thermo Scientific LTQ Orbitrap XL mass spectrometer (Thermo Fisher Scientific Inc., Waltham, MA). Semi-preparative high-performance liquid chromatography (HPLC) was run on with a Shimadzu LC-20AP system equipped with a Shimadzu SPD-20A dual wavelength detector (Shimadzu Corporation, Tokyo, Japan) and a YMC C₁₈ column (10 mm \times 250 mm, 5 μm) (YMC Co. Ltd., Kyoto, Japan). Column chromatography was done with silica gel (Qingdao marine Chemical Co. Ltd., Qingdao, China), ODS (40–60 μm , Fuji, Silysia Chemical Ltd., Japan), Sephadex LH-20 (Amersham Pharmacia Biotech Co. Ltd., Tokyo, Japan). Inhibitory activities were tested on a multi-mode microplate reader

(Synergy HTX, BioTek Instruments Inc., USA). α -Glucosidase (EC 3.2.1.20), 1-deoxynojirimycin, genistein, NG-monomethyl-L-arginine (L-NMMA) and lipopolysaccharide (LPS) were provided by Sigma-Aldrich Chemical Company (St. Louis, MO, USA), and *p*-nitrophenyl- α -D-glucopyranoside (*p*NPG) was purchased from Macklin Biochemical Co. Ltd. (Shanghai, China).

Plant Materials. The rhizomes of *A. villosum* var. *xanthioides* were collected in April 2016 from Yunnan province of China. They were authenticated by Professor S.C. Zhang, Department of Medicinal Plants, Xishuangbanna Tropical Botanical Garden. A voucher specimen (No. 160416) is deposited in the Laboratory of Natural Product Chemistry, Northwest A&F University.

Extraction and Isolation. The air-dried rhizomes of *A. villosum* var. *xanthioides* (10 kg) were extracted with 95 % EtOH (3 \times 4 h). The EtOH extract (460 g) was suspended in H₂O, and then successively partitioned with petroleum ether (PE), CH₂Cl₂ and EtOAc, yielding fractions of PE (100 g), CH₂Cl₂ (64 g) and EtOAc (25 g) after removal of the solvent, respectively. The PE fraction was subjected to silica gel column chromatography (CC), using gradient elution of PE/EtOAc (100:1, 50:1, 20:1, 10:1, 5:1, 1:1), to yield five major fractions (Fr.1–Fr.5) by their TLC profiles. The Fr.4 was performed on Sephadex LH-20 CC, eluting with CH₂Cl₂/MeOH (1:1), to obtain Fr.4.1–Fr.4.3. The Fr.4.3 was then applied to CC over ODS with a step gradient of MeOH/H₂O (30:70 to 90:10), to afford four subfractions (Fr.4.3.1–Fr.4.3.4). The Fr.4.3.4 was separated by silica gel CC with PE/acetone/MeOH (10:1:0.1) as an eluent, and further purified by semi-preparative HPLC with MeOH/H₂O (78:22) as a mobile phase to give **2** (2.1 mg). The Fr.3 was subjected to CC over D101 eluting with varying gradients of EtOH/H₂O (30:70 to 100:0), to give five subfractions (Fr.3.1–Fr.3.5) according to the TLC analysis. The Fr.3.2 was subjected to Sephadex LH-20 CC using CH₂Cl₂/MeOH (1:1) as an eluent, and then Fr.3.2.2 was separated by an ODS column with a

continuous gradient of MeOH/H₂O (30:70 to 100:0), to afford two major subfractions Fr.3.2.2.3 and Fr.3.2.2.4. The Fr.3.2.2.3 was chromatographed on a silica gel column (PE/acetone/MeOH = 10:1:0.1), and purified by semi-preparative HPLC using MeOH/H₂O (78:22), to obtain **4** (4.0 mg) and **11** (2.7 mg). Fr.3.2.2.4 was performed on CC over silica gel with a gradient elution of PE/acetone/MeOH (15:1:0.01, 5:1:0.1) to yield Fr.3.2.2.4.1 and Fr.3.2.2.4.2. Separation of Fr.3.2.2.4.1 was carried out by semi-preparative HPLC with MeOH/H₂O (78:22), giving **12** (0.8 mg). Meanwhile, Fr.3.2.2.4.2 was purified by semi-preparative HPLC eluting with MeOH/H₂O (80:20) to afford **3** (0.8 mg). The Fr.3.3 was applied to CC over Sephadex LH-20 (CH₂Cl₂/MeOH = 1:1) and ODS with gradient of MeOH/H₂O (30:70 to 90:10). The subfractions eluted with MeOH/H₂O (90:10) on the ODS column were collected, and Fr.3.3.2 was further separated by silica gel CC (PE/acetone/MeOH = 18:1:0.1), to obtain Fr.3.3.2.2. The Fr.3.3.2.2 was performed on semi-preparative HPLC with MeOH/H₂O (82:18), to afford **6** (8.7 mg) and **5** (0.9 mg). In the same way, the Fr.2 was first eluted with a gradient of increasing EtOH (10%–100%) in water on a D101 column to gain four subfractions (Fr.2.1–Fr.2.4). The Fr.2.2 was applied to Sephadex LH-20 CC (CH₂Cl₂/MeOH = 1:1), followed by silica gel CC with an eluent of PE/acetone/MeOH (30:1:0.08), and Fr.2.2.2 obtained was then chromatographed on semi-preparative HPLC with MeOH/H₂O (78:22), to give **1** (3.3 mg). The Fr.2.3 was then subjected to Sephadex LH-20 CC with an eluent of CH₂Cl₂/MeOH (1:1), and further separated by repeated CC over ODS, to give Fr.2.3.1. The two subfractions, Fr.2.3.1.1 and Fr.2.3.1.2, were obtained from Fr.2.3.1 with silica gel CC (PE/acetone/MeOH = 50:1:0.1). The following purification of the above subfractions (Fr.2.3.1.1 and Fr.2.3.1.2) were achieved by semi-preparative HPLC with the same mobile phase of MeOH/H₂O (84:16), yielding **9** (2.8 mg), **10** (1.0 mg) and **8** (6.8 mg) from Fr.2.3.1.1, and **7** (3.3 mg) from

Fr.2.3.1.2, respectively.

Avxanthin A (1): Colorless oil; $[\alpha]^{25}_{\text{D}} +35.1$ (*c* 0.03, MeOH); UV (MeOH) λ_{max} ($\log \epsilon$) 237 (3.96) nm; CD (*c* 1.10×10^{-4} , MeOH) λ_{max} ($\Delta\epsilon$) 242 (+5.01), 312(−4.25) nm; ^1H (500 MHz) and ^{13}C NMR (125 MHz) data, see Table 1; HRESIMS m/z 233.1899 $[\text{M} + \text{H}]^+$ (calcd for $\text{C}_{16}\text{H}_{25}\text{O}$, 233.1899).

Avxanthin B (2): White powder; $[\alpha]^{25}_{\text{D}} +74.2$ (*c* 0.03, MeOH); UV (MeOH) λ_{max} ($\log \epsilon$) 230 (4.18) nm; ^1H (500 MHz) and ^{13}C NMR (125 MHz) data, see Table 2; HRESIMS m/z 317.2114 $[\text{M} + \text{H}]^+$ (calcd for $\text{C}_{20}\text{H}_{29}\text{O}_3$, 317.2111).

Avxanthin C (3): Colorless oil; $[\alpha]^{25}_{\text{D}} +62.8$ (*c* 0.04, MeOH); UV (MeOH) λ_{max} ($\log \epsilon$) 222 (4.10) nm; ^1H (500 MHz) and ^{13}C NMR (125 MHz) data, see Table 2; HRESIMS m/z 363.2531 $[\text{M} + \text{H}]^+$ (calcd for $\text{C}_{22}\text{H}_{35}\text{O}_4$, 363.2530).

(5S,9S,10S,16R,11E)-16-Hydroxyabda-8(17),11,13-trien-15,16-olide (4): Yellowish oil; $[\alpha]^{25}_{\text{D}} +45.8$ (*c* 0.03, MeOH); UV (MeOH) λ_{max} ($\log \epsilon$) 261 (4.36) nm; CD (*c* 1.10×10^{-4} , MeOH) λ_{max} ($\Delta\epsilon$) 260 (+5.26) nm; ^1H (500 MHz) and ^{13}C NMR (125 MHz) data, see Table 2; HRESIMS m/z 317.2112 $[\text{M} + \text{H}]^+$ (calcd for $\text{C}_{20}\text{H}_{29}\text{O}_3$, 317.2111).

ECD Calculation Methods. Conformational analysis were performed with the MMFF force field (Merck Molecular force field) using the Monte Carlo algorithm implemented in Spartan'18 (Wavefunction, Irvine, CA, USA, 2018) using default parameters and convergence criteria. All minima thus found were optimized with DFT method first at $\omega\text{B97X-D/6-31G(d)}$ and then at $\omega\text{B97X-D/6-311G+(d,p)}$ level of theory in Spartan'18, using default grids and convergence criteria. Finally, all minima with relative energies within 5 kcal/mol from the lowest energy minima were re-optimized at $\omega\text{B97X-D/6-311G+(d,p)}$ level of theory including SMD solvent model for methanol, using Gaussian'16 package (revision A.03; Gaussian Inc.: Wallingford, CT, USA, 2016), using

default grids and convergence criteria. The above steps produced only one conformer for compound **1**, eight conformers for compound **2** and four conformers for compound **4** (for each of the two possible diastereomers).

Excited state calculations were run with Gaussian'16 with the time-dependent density functional theory (TD-DFT) method using CAM-B3LYP and B3LYP functionals, def2-TZVP basis set, and IEF-PCM solvent model for methanol. The 24 lowest electronic transitions (roots) were included in the calculations. ECD spectra of the conformers were simulated by using a Gaussian function with a half-bandwidth of 0.35-0.40 eV. The overall theoretical ECD spectra were obtained according to the Boltzmann weighting of each conformer, using internal energies. ECD spectra were plotted using the program SpecDis (version 1.71; Berlin: Germany, 2017; <http://specdis-software.jimdo.com>). Similarity factors were evaluated with the same software.

Anti-inflammatory assay. The bioassays for NO production and cell viability were conducted by the reported methods,³⁰ and NG-monomethyl-L-arginine (L-NMMA) was used as the positive control.

Molecular Docking Simulation. Molecular docking was performed according to the previously published paper.³⁵

α -Glucosidase Inhibitory Activity. Inhibitory activities of α -glucosidase and inhibition kinetics were conducted following the methods reported previously, using 1-deoxynojirimycin and genistein as positive controls.^{33,34}

ASSOCIATED CONTENT

Supporting Information

The Supporting Information is available free of charge on the ACS Publications website.

Lineweaver–Burk equation, secondary equations acquired from the Lineweaver–Burk equation; the Michaelis–Menten plots, the kinetic parameters; 1D NMR, 2D NMR and HRESIMS spectra of compounds **1–4** (PDF)

AUTHOR INFORMATION

Corresponding Author

*Telephone: + 86-29-87092335. E-mail: jinminggao@nwsuaf.edu.cn

ORCID

Jin-Ming Gao: 0000-0003-4801-6514

Gennaro Pescitelli: 0000-0002-0869-5076

Notes

The authors declare no competing financial interest.

ACKNOWLEDGMENTS

This research was supported by the National Natural Science Foundation of China (No. 31600275 and 31800281), the Doctoral Starting Fund of Xinxiang Medical University (XYBSKYZZ201813).

G.P. acknowledges the CINECA award under the ISCRA initiative for the availability of high-performance computing resources and support.

REFERENCES

- (1) Flora of China Editorial Committee. Flora Reipublicae Popularis Sinicae (Zhongguo Zhiwu Zhi); Science Press: Beijing, China, 1981; *16*(2), pp 125.
- (2) Chinese Pharmacopoeia Commission. Pharmacopoeia of the People's Republic of China 2010; China Medical Science and Technology Press: Beijing, China, 2010; *1*, pp 236–237.
- (3) State Administration of TCM of China Editorial Committee. Chinese Materia Medica-Dai

medicine volume. Shanghai Science & Technology Press: Shanghai, China, 2005; pp 270–271.

- (4) Ye, Q.; Li, S. M.; Ao, H.; Chen, L.; Li, H. X. *Chinese Traditional Patent Medicine* **2014**, *36*, 1033–1037 (in Chinese).
- (5) Choi, J. W.; Kim, K. H.; Lee, H. K.; Choi, S. U.; Lee, K. R. *Nat. Prod. Sci.* **2009**, *15*, 44–49.
- (6) Kim, K. H.; Choi, J. W.; Choi, S. U.; Lee, K. R. *Planta Med.* **2010**, *76*, 461–464.
- (7) Lee, Y. S.; Kang, M. H.; Cho, S. Y.; Jeong, C. S. *Arch. Pharm. Res.* **2007**, *30*, 436–443.
- (8) Kim, S. H.; Shin, T. Y. *Exp. Biol. Med.* **2005**, *230*, 681–687.
- (9) Kim, S. H.; Lee, S.; Kim, I. K.; Kwon, T. K.; Moon, J. Y.; Park, W. H.; Shin, T. Y. *Food Chem. Toxicol.* **2007**, *45*, 2138–2144.
- (10) Wang, J. H.; Wang, J.; Choi, M. K.; Gao, F.; Lee, D. S.; Han, J. M.; Son, C. G. *Pharm. Biol.* **2013**, *51*, 930–935.
- (11) Yin, H.; Luo, J. G.; Kong, L. Y. *J. Nat. Prod.* **2013**, *76*, 237–242.
- (12) Luo, J. G.; Yin, H.; Fan, B. Y.; Kong, L. Y. *Helv. Chim. Acta* **2014**, *97*, 1140–1145.
- (13) Yin, H.; Luo, J. G.; Shan, S. M.; Wang, X. B.; Luo, J.; Yang, M. H.; Kong, L. Y. *Org. Lett.* **2013**, *15*, 1572–1575.
- (14) Gawronski, J. Conformations, chiroptical and related spectral properties of enones. In: Patai, S.; Rappoport, Z.; editors. *The chemistry of enones*. Chichester, England: Wiley, 1989; Chap 3, pp 55–105.
- (15) Hassan, Z.; Hussain, H.; Ahmad, V. U.; Anjum, S.; Pescitelli, G.; Kurtán, T.; Krohn, K. *Tetrahedron: Asymmetry* **2007**, *18*, 2905–2909.
- (16) Pescitelli, G.; Bruhn, T. *Chirality* **2016**, *28*, 466–474.
- (17) Superchi, S.; Scafato, P.; Górecki, M.; Pescitelli, G. *Curr. Med. Chem.* **2018**, *25*, 287–320.

- (18) Kong, L. Y.; Qin, M. J.; Niwa, M. *J. Nat. Prod.* **2000**, *63*, 939–942.
- (19) Chimnoi, N.; Pisutjaroenpong, S.; Ngiwsara, L.; Dechtrirut, D.; Chokchaichamnankit, D.; Khunnawutmanotham, N.; Mahidol, C.; Techasakul, S. *Nat. Prod. Res.* **2008**, *22*, 1249–1256.
- (20) Schramm, A.; Ebrahimi, S. N.; Raith, M.; Zaugg, J.; Rueda, D. C.; Hering, S.; Hamburger, M. *Phytochemistry* **2013**, *96*, 318–329.
- (21) Mohamad, H.; Lajis, N. H.; Abas, F.; Ali, A. M.; Sukari, M. A.; Kikuzaki, H.; Nakatani, N. *J. Nat. Prod.* **2005**, *68*, 285–288.
- (22) Akiyama, K.; Kikuzaki, H.; Aoki, T.; Okuda, A.; Lajis, N. H.; Nakatani, N. *J. Nat. Prod.* **2006**, *69*, 1637–1640.
- (23) Braun, M.; Hohmann, A.; Rahematpura, J.; Bühne, C.; Grimme, S. *Chem. Eur. J.* **2004**, *10*, 4584 – 4593.
- (24) Villamizar, J.; Pittelaud, J. P.; Rodrigues, J. R.; Gamboa, N.; Canudas, N.; Tropper, E.; Salazar, F.; Fuentes, J. *Nat. Prod. Res.* **2009**, *23*, 891–902.
- (25) Singh, S.; Gray, A. I.; Waterman, P. G. *Nat. Prod. Lett.* **1993**, *3*, 163–166.
- (26) Singh, S.; Gray, A. I.; Skelton, B. W.; Waterman, P. G.; White, A. H. *Aust. J. Chem.* **1991**, *44*, 1789–1793.
- (27) Villamizar, J. E.; Juncosa, J.; Pittelaud, J.; Hernández, M.; Canudas, N.; Tropper, E.; Salazar, F.; Fuentes, J. *J. Chem. Res.* **2007**, *31*, 342–346.
- (28) Sivasothy, Y.; Ibrahim, H.; Paliany, A. S.; Alias, S. A.; Md. Nor, N. R.; Awang, K. *Planta Med.* **2013**, *79*, 1775–1780.
- (29) Waters, S. P.; Tian, Y.; Li, Y. M.; Danishefsky, S. J. *J. Am. Chem. Soc.* **2005**, *127*, 13514–13515.

- (30) Li, J., Zhao, F., Li, M.Z., Chen, L.X., Qiu, F., 2010. *J. Nat. Prod.* 2010, 73, 1667–1671.
- (31) Wang, P.; Xie, C.; An, L.; Yang, X.; Xi, Y.; Yuan, S.; Zhang, C.; Tuerhong, M.; Jin, D. Q.; Lee, D.; Zhang, J.; Ohizumi, Y.; Xu, J.; Guo, Y. *J. Nat. Prod.* **2019**, 82, 183–193.
- (32) Wang, P.; Liu, F.; Yang, X.; Liang, Y.; Li, S.; Su, G.; Jin, D. Q.; Ohizumi, Y.; Xu, J.; Guo, Y. *Phytochemistry* **2017**, 144, 141–150.
- (33) Hu, X. J.; Wang, X. B.; Kong, L. Y. *J. Agric. Food Chem.* **2013**, 61, 1501–1508.
- (34) Ding, H.; Wu, X.; Pan, J.; Hu, X.; Gong, D.; Zhang, G. *J. Agric. Food Chem.* **2018**, 66, 7065–7075.
- (35) Tang, D.; Liu, L. L.; He, Q. R.; Yan, W.; Li, D.; Gao, J. M. *J. Nat. Prod.* **2018**, 81, 1984–1991.

Captions for tables and figures

Table 1. ^1H and ^{13}C NMR Data of Compound **1** in CDCl_3

Table 2. ^1H and ^{13}C NMR Data of Compounds **2–4**

Table 3. Inhibitory Activities on NO Production Induced by LPS in Macrophages

Table 4. Inhibitory Activities on α -Glucosidase^a

Figure 1. Chemical structures of compounds **1–12**.

Figure 2. Key HMBC, ^1H - ^1H COSY and ROESY correlations of compound **1**.

Figure 3. Experimental CD spectrum of (+)-**1** in MeOH compared with the spectrum calculated on (5*S*,10*R*)-**1** at the TD-CAM-B3LYP/def2-TZVP// ω B97X-D/6-31+G(d,P) level, including PCM solvent model for MeOH. Plotting parameters: Gaussian band-width 0.4 eV, wavelength shift +19 nm, scaled by a factor 1.3.

Figure 4. Key HMBC and ROESY correlations of compounds **2–4**.

Figure 5. Left: Experimental CD spectrum of (+)-**2** in MeOH compared with the spectra calculated on (5*S*,9*S*,10*S*)-**2** at the TD-CAM-B3LYP/ def2-TZVP// ω B97X-D/6-31+G(d) level, including PCM solvent model for MeOH. Plotting parameters: Gaussian band-width 0.35 eV, wavelength shift 10 nm, scaled by a factor 0.5. Right: DFT-optimized structures for the lowest-energy conformers of **2**, with diagnostic NOE's indicated.

Figure 6. Experimental CD spectrum of (+)-**4** in MeOH compared with the spectra calculated on (5*S*,9*S*,10*S*,16*R*)-**4** and (5*S*,9*S*,10*S*,16*S*)-**4** (epi-**4**) at the TD-CAM-B3LYP/def2-TZVP// ω B97X-D/6-31+G(d) level, including PCM solvent model for MeOH. Plotting parameters: Gaussian band-width 0.4 eV, wavelength shift 0 nm, scaled by a factor 5.

Figure 7. Molecular docking simulation of compound **4** (carbon atom in orchid) with iNOS (PDB:

3E7G).

Figure 8. Lineweaver–Burk plots. α -Glucosidase was treated with various concentrations of *p*NPG in the absence or presence of compound **4** (0, 10, 20 μ M).

Scheme 1. Plausible Biogenetic Pathway of Compound **1**

Table 1. ^1H and ^{13}C NMR Data of Compound **1** in CDCl_3

no.	δ_{C} type	δ_{H} (<i>J</i> in Hz)
1	42.0 CH ₂	1.64 br d (15.0) 1.20 m ^a
2a	18.9 CH ₂	1.58 tt (15.0, 5.0)
2b		1.46 dq (15.0, 5.0)
3	42.8 CH ₂	1.48 dq (15.0, 5.0) 1.22 m ^a
4	33.3 C	
5	48.8 CH	1.21 dd (10.0, 5.0)
6a	18.8 CH ₂	2.34 br d (15.0)
6b		1.89 br t (15.0)
7	138.5 C	
8	172.6 C	
9a	48.9 CH ₂	2.16 d (15.0)
9b		2.00 d (15.0)
10	33.9 C	
11	30.1 CH ₂	2.43 br t (15.0) 2.40 m ^a
12	35.0 CH ₂	2.39 dd (10.0, 5.0)
13	209.3 C	
14	33.1 CH ₃	0.911 s
15	21.7 CH ₃	0.915 s
16	19.8 CH ₃	0.85 s

^aOverlapped signals.

Table 2. ^1H and ^{13}C NMR Data of Compounds **2–4**

no.	2^a		3^a		4^b	
	δ_{C} type	δ_{H} (J in Hz)	δ_{C} type	δ_{H} (J in Hz)	δ_{C} type	δ_{H} (J in Hz)
1	39.5 CH ₂	1.70 br d (12.5) 1.08 ddd (12.5, 12.5, 3.5)	39.5 CH ₂	1.70 br d (14.0) 1.07 t (12.5)	42.0 CH ₂	1.46 m ^c 1.10 br t (13.5)
2	19.5 CH ₂	1.59 m 1.52 m	19.5 CH ₂	1.58 m 1.51 br d (12.0)	20.1 CH ₂	1.59 qt (13.5, 2.0) 1.44 m ^c
3	42.1 CH ₂	1.42 br d (13.0) 1.20 ddd (13.0, 13.0, 4.0)	42.3 CH ₂	1.41 d (13.5) 1.19 br t (12.5)	43.3 CH ₂	1.43 m ^c 1.24 br t (13.0)
4	33.7 C		33.8 C		34.5 C	
5	55.6 CH	1.12 dd (12.5, 2.0)	55.6 CH	1.12 d (12.5)	55.8 CH	1.18 dd (12.5, 2.5)
6 α	24.2 CH ₂	1.74 br d (13.0)	24.3 CH ₂	1.73 br d (17.0)	24.5 CH ₂	1.76 ddt (13.0, 5.0, 2.5)
6 β		1.34 qd (13.0, 4.0)		1.33 br d (13.5)		1.41 m ^c
7	37.9 CH ₂	2.40 br d (13.0) 2.00 ddd (13.0, 12.7, 4.5)	38.1 CH ₂	2.39 m ^c 2.02 br t (10.5)	37.7 CH ₂	2.46 ddt (13.5, 4.0, 2.0) 2.12 td (13.5, 5.0)
8	148.2 C		148.4 C		150.3 C	
9	56.4 CH	1.87 br d (11.0)	56.6 CH	1.88 d (11.0)	63.3 CH	2.53 d (10.0)
10	39.7 C		39.7 C		40.5 C	
11	25.3 CH ₂	2.35 dd (15.0, 4.5) 2.21 m	24.6 CH ₂	2.42 m ^c 2.24 m	144.6 CH	6.62 dd (16.0, 10.0)
12	141.6 CH	6.80 t (7.0)	149.8 CH	7.01 t (6.0)	124.3 CH	6.38 d (16.0)
13	125.9 C		124.3 C		163.9 C	
14	33.3 CH ₂	3.26 s	32.7 CH ₂	3.35 s	116.1 CH	5.91 s
15	173.9 C		170.7 C		173.8 C	
16	169.6 C		169.8 C		99.9 CH	6.30 s
17	107.6 CH ₂	4.84 s 4.38 s	108.0 CH ₂	4.84 s 4.40 s	109.1 CH ₂	4.78 d (1.0) 4.49 br s
18	33.7 CH ₃	0.89 s	33.8 CH ₃	0.88 s	34.0 CH ₃	0.92 s
19	21.9 CH ₃	0.82 s	21.9 CH ₃	0.82 s	22.4 CH ₃	0.88 s
20	14.5 CH ₃	0.73 s	14.6 CH ₃	0.72 s	15.5 CH ₃	0.91 s
21			61.1 CH ₂	4.16 q (7.0)		
22			14.3 CH ₃	1.26 t (7.0)		

^aMeasured in CDCl₃. ^bMeasured in CD₃OD. ^cOverlapped signals.

Table 3. Inhibitory Activities on NO Production Induced by LPS in Macrophages

compound	IC ₅₀ (μ M) ^a
1	43.06 \pm 1.37
2	11.02 \pm 0.75
3	> 50
4	2.36 \pm 0.86
5	18.84 \pm 1.06
6	30.79 \pm 0.98
7	24.61 \pm 1.12
8	31.20 \pm 0.76
9	25.83 \pm 0.93
10	> 50
11	23.68 \pm 1.36
12	28.73 \pm 0.77
L-NMMA	27.23 \pm 0.56

^aResults were expressed as means \pm SD (n = 3).

Table 4. Inhibitory Activities on α -Glucosidase^a

compound	inhibition ratio (%) ^b	IC ₅₀ (μ M)
1	12.36 \pm 0.59	> 50
2	90.33 \pm 1.22	21.08 \pm 0.69
3	38.66 \pm 1.09	> 50
4	95.70 \pm 0.56	9.98 \pm 0.67
5	88.99 \pm 0.91	14.78 \pm 0.94
6	89.09 \pm 0.47	17.11 \pm 0.53
7	87.85 \pm 1.17	15.80 \pm 0.80
8	89.33 \pm 0.37	13.77 \pm 0.52
9	87.36 \pm 1.19	17.52 \pm 1.02
10	36.90 \pm 0.89	> 50
11	33.22 \pm 0.61	> 50
12	27.06 \pm 0.52	> 50
1-deoxynojirimycin	36.85 \pm 1.51	114.88 \pm 0.96
genistein	70.04 \pm 0.85	17.61 \pm 0.44

^aResults were expressed as means \pm SD (n = 3). ^bPercent inhibition at a concentration of 50 μ M.

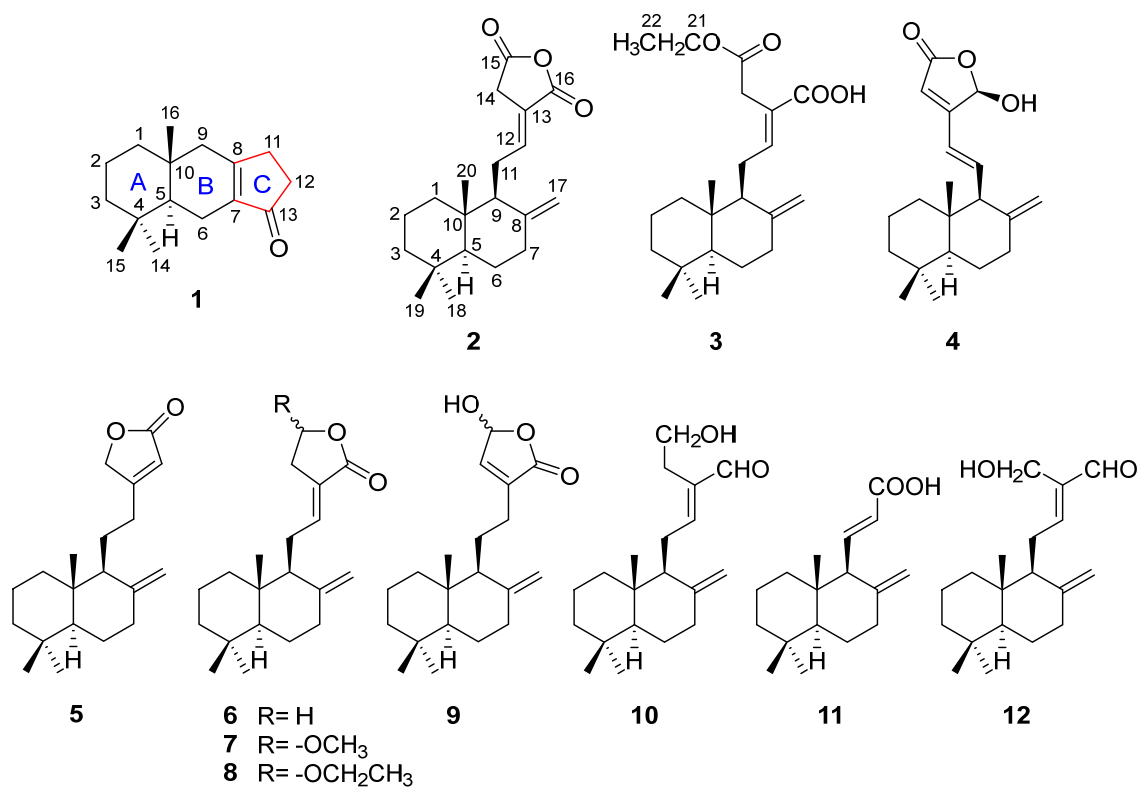


Figure 1. Chemical structures of compounds 1–12.

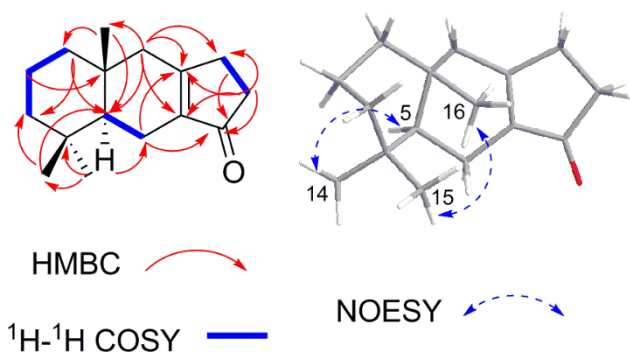


Figure 2. Key HMBC, ^1H - ^1H COSY and ROESY correlations of compound **1**.

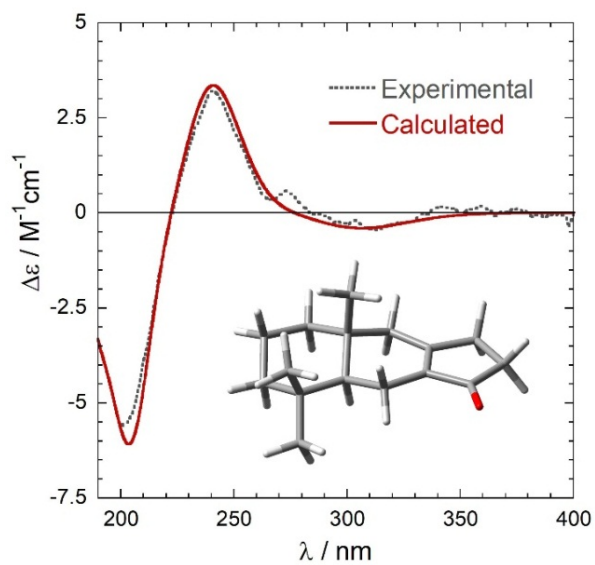


Figure 3. Experimental CD spectrum of (+)-**1** in MeOH compared with the spectrum calculated on (5*S*,10*R*)-**1** at the TD-CAM-B3LYP/def2-TZVP// ω B97X-D/6-31+G(d,P) level, including PCM solvent model for MeOH. Plotting parameters: Gaussian band-width 0.4 eV, wavelength shift +19 nm, scaled by a factor 1.3.

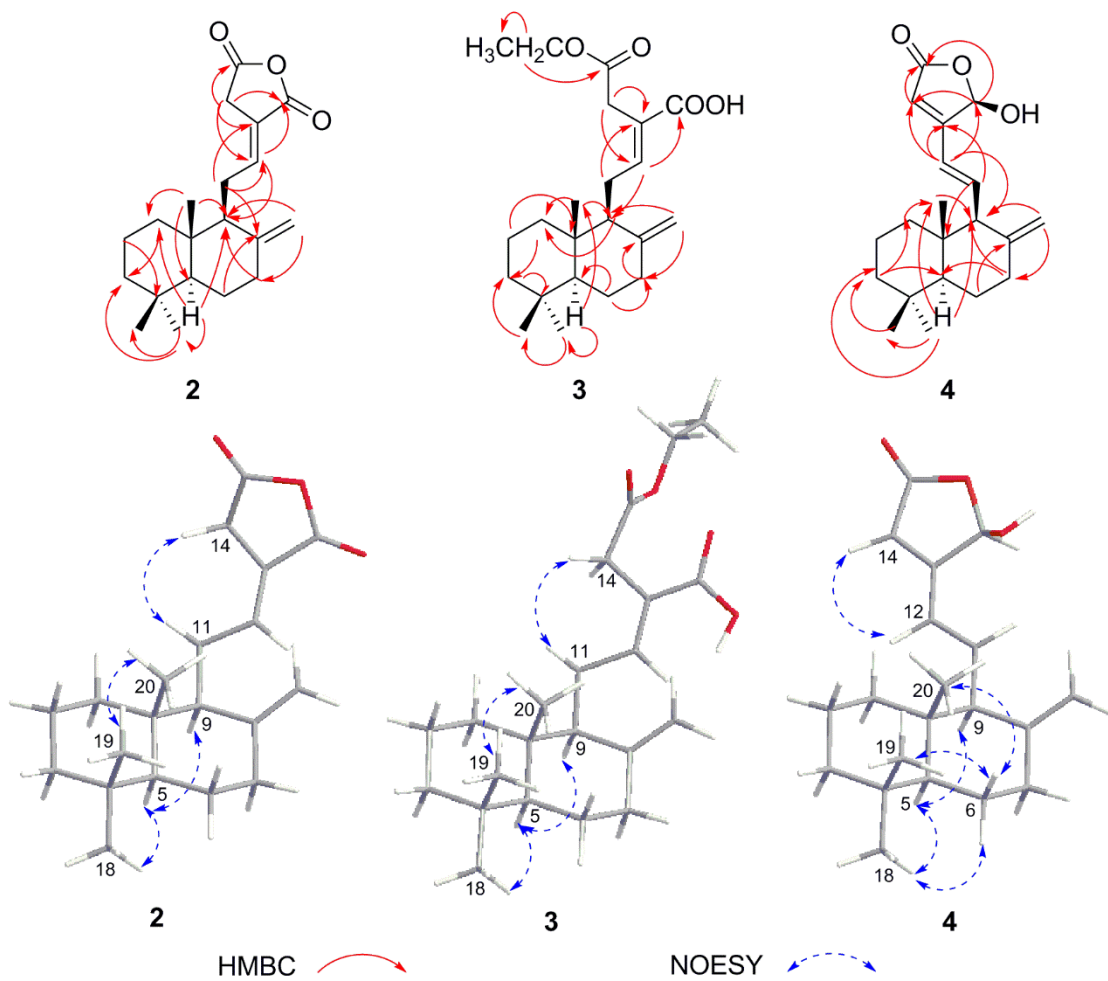


Figure 4. Key HMBC and ROESY correlations of compounds 2–4.

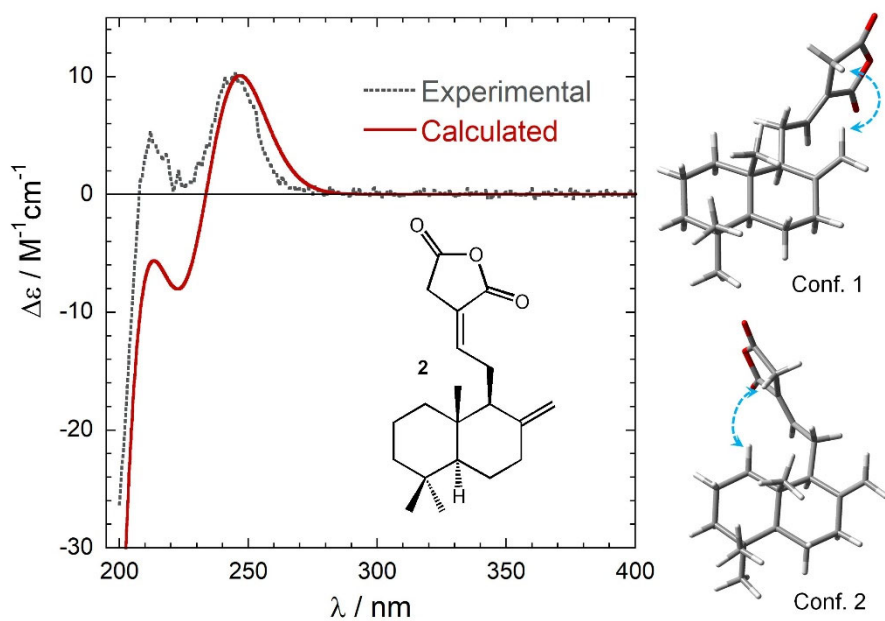


Figure 5. Left: Experimental CD spectrum of (+)-**2** in MeOH compared with the spectra calculated on (5*S*,9*S*,10*S*)-**2** at the TD-CAM-B3LYP/ def2-TZVP// ω B97X-D/6-31+G(d) level, including PCM solvent model for MeOH. Plotting parameters: Gaussian band-width 0.35 eV, wavelength shift 10 nm, scaled by a factor 0.5. Right: DFT-optimized structures for the lowest-energy conformers of **2**, with diagnostic NOE's indicated.

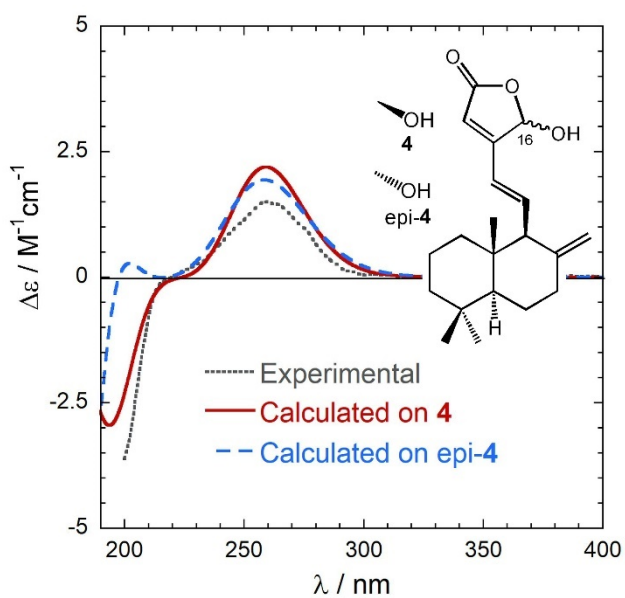


Figure 6. Experimental CD spectrum of (+)-**4** in MeOH compared with the spectra calculated on (5*S*,9*S*,10*S*,16*R*)-**4** and (5*S*,9*S*,10*S*,16*S*)-**4** (epi-**4**) at the TD-CAM-B3LYP/def2-TZVP// ω B97X-D/6-31+G(d) level, including PCM solvent model for MeOH. Plotting parameters: Gaussian band-width 0.4 eV, wavelength shift 0 nm, scaled by a factor 5.

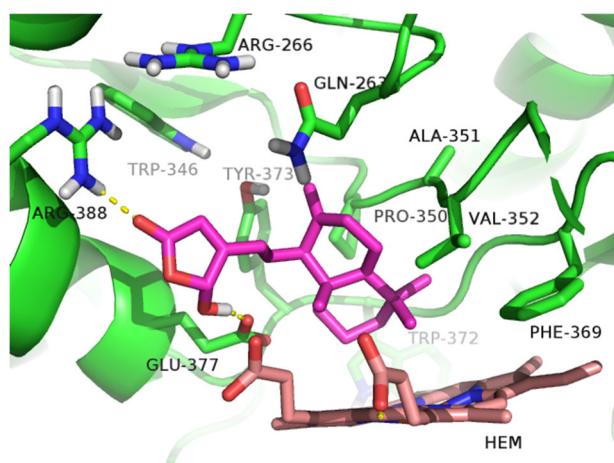


Figure 7. Molecular docking simulation of compound 4 (carbon atom in orchid) with iNOS (PDB: 3E7G).

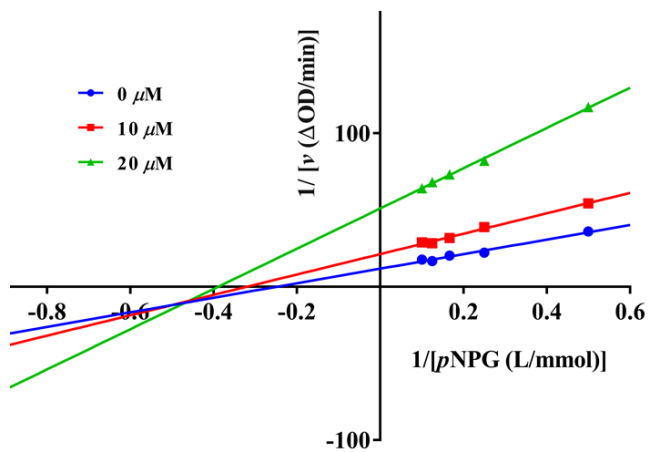
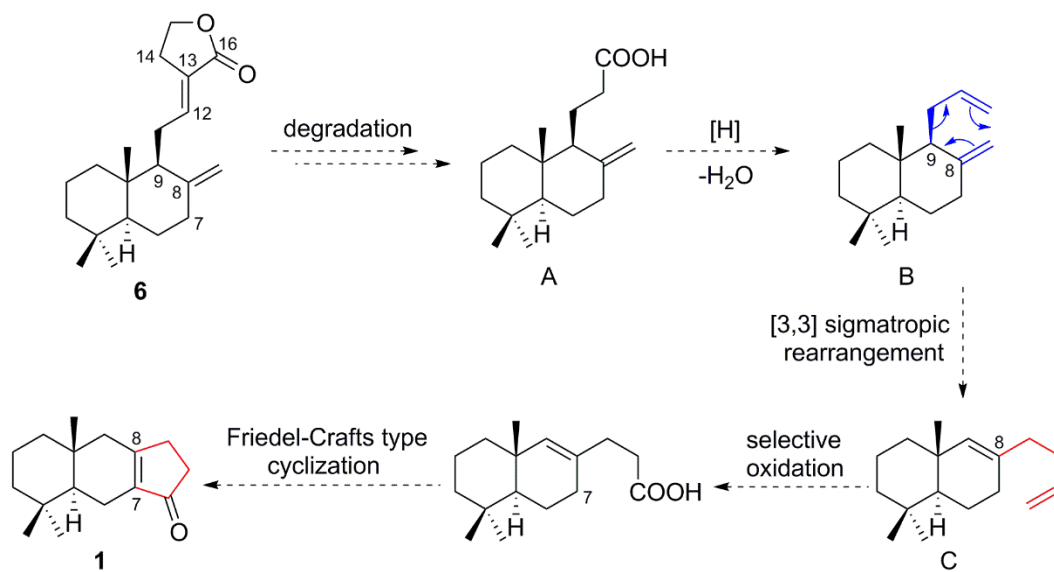


Figure 8. Lineweaver–Burk plots. α -Glucosidase was treated with various concentrations of *p*NPG in the absence or presence of compound 4 (0, 10, 20 μM).

Scheme 1. Plausible Biogenetic Pathway of Compound 1



Graphic for table of contents

